JOURNAL OF GUIDANCE, CONTROL, AND DYNAMICS
Vol. 30, No. 3, May–June 2007

Stability and Control of a High-Altitude, Long-Endurance UAV

Ilhan Tuzcu*
University of Alabama, Tuscaloosa, Alabama 35487-0280
Pier Marzocca†
Clarkson University, Potsdam, New York 13699-5725
and
Enrico Cestino,‡ Giulio Romeo,§ and Giacomo Frulla¶
Politecnico di Torino, Turin, 10129, Italy

DOI: 10.2514/1.25814

This paper addresses stability analysis, control design, and simulation of high-altitude, long-endurance unmanned aerial vehicles. These aircraft are highly flexible and have very low structural frequencies. Hence, the separation between the elastic and rigid body motions no longer exists, and an approach that unifies these two motions must be used. The available data of the aircraft considered include the geometry of the aircraft, aerodynamic data, and mass, flexural rigidity, and torsional rigidity distributions. The wing of the aircraft is modeled as a flexible beam undergoing bending and torsion, whereas the remaining members are assumed to be rigid. The equations of motion are obtained by means of the Lagrangian equations in quasi coordinates. A perturbation approach separates the problem into *nominal dynamics* and *perturbation dynamics*. The equations for nominal dynamics are used to design desired maneuvers and to determine the corresponding structural deformations. The equations for perturbation dynamics are used to address stability of the aircraft on the desired flight paths, to design feedback controls to maintain stable flights, and to simulate the motion of the aircraft.

Nomenclature

A, B	=	system matrices
C	=	matrix of direction cosines between the inertial and body axes
C_i	=	matrix of direction cosines for the body axes of component i
C_{La}, C_{Le}, C_{Lr}	=	control effectiveness for the aileron, elevator, and rudder
$C_{L\alpha}$	=	lift curve slope
C_{L0}	=	lift coefficient at zero angle of attack
c_i	=	aerodynamic chord for component i
D_r, D_l	=	damping matrices for bending
$\mathcal{D}_r$, $\mathcal{D}_l$	=	damping matrices for torsion
d_i	=	drag force per unit span of component i
E	=	matrix relating Eulerian velocities to angular velocities
$\boldsymbol{F}$, $\boldsymbol{M}$	=	resultant force and moment vectors
$\boldsymbol{f}_{ai}$, $\boldsymbol{f}_{gi}$	=	distributed aerodynamic and gravity force vectors for body i
G	=	control gain matrix
g	=	gravity constant
I	=	identity matrix
J	=	second moment of inertia matrix
K	=	Riccati matrix
K_r, K_l	=	stiffness matrices for bending
$\mathcal{K}_r$, $\mathcal{K}_l$	=	stiffness matrices for torsion
ℓ	=	length of the half-wing
l_i	=	lift force per unit span of component i
M	=	discrete system mass matrix
$\mathcal{M}$	=	Mach number
m	=	total aircraft mass
m_i	=	mass of component i
O	=	origin of inertial axes
o	=	origin of body axes
o_i	=	origin of body axes of component i
$\boldsymbol{p}_i$, $\boldsymbol{\rho}_i$	=	momentum vectors of component i for bending and torsion
$\boldsymbol{p}_v$, $\boldsymbol{\rho}_\omega$	=	linear and angular momentum vectors
$\boldsymbol{Q}_i$	=	generalized force vector of component i for bending
q_i	=	local dynamic pressure for component i
$\boldsymbol{q}_i$	=	vector of generalized coordinates of component i for bending
$\boldsymbol{R}$	=	position vector of o relative to O
$\boldsymbol{r}_i$	=	nominal position vector of a point relative to o_i
$\tilde{S}$	=	matrix of first moment of inertia
$\boldsymbol{s}_i$	=	vector of generalized velocities of component i for bending
T	=	total kinetic energy
$\boldsymbol{T}$	=	engine thrust
T_i	=	kinetic energy of component i
U_i	=	matrix of shape functions of component i for bending
$\boldsymbol{u}_i$, $\boldsymbol{v}_i$	=	elastic displacement and velocity vectors for component i
$\boldsymbol{v}$, $\boldsymbol{\omega}$	=	rigid body translational and angular velocity vectors
$\bar{\boldsymbol{v}}_i$	=	velocity vector of a point on component i
XYZ	=	inertial axes
$\boldsymbol{x}$	=	state vector
xyz	=	body axes of the whole aircraft
$x_i y_i z_i$	=	body axes of component i

Presented as Paper 1641 at the 47th AIAA/ASME/ASCE/AHS/ASC Structures, Structural Dynamics, and Materials Conference, Newport, RI, 1–4 May 2006; received 12 June 2006; revision received 27 November 2006; accepted for publication 2 December 2006.

*Assistant Professor, Department of Aerospace Engineering and Mechanics; ituzcu@eng.ua.edu.

†Assistant Professor, Department of Mechanical and Aeronautical Engineering, CAMP 234; pmarzocc@clarkson.edu.

‡Researcher, Department of Aerospace Engineering; enrico.cestino@polito.it.

§Professor, Department of Aerospace Engineering; giulio.romeo@polito.it.

¶Associate Professor, Department of Aerospace Engineering; giacomo.frulla@polito.it.

$\boldsymbol{y}$ = state vector for quasi-rigid aircraft
$\boldsymbol{z}$ = state vector for restrained aircraft
α_i = local angle of attack of component i
$\delta_a, \delta_e, \delta_r$ = aileron, elevator, and rudder angles
$\boldsymbol{\eta}_i$ = vector of generalized velocities of component i for torsion
$\boldsymbol{\theta}$ = vector of Euler angles
$\boldsymbol{\Theta}_i$ = generalized force vector of component i for torsion
$\boldsymbol{\xi}_i$ = vector of generalized coordinates of component i for torsion
ρ = air density
ϕ, θ, ψ = Euler angles (roll, pitch, and yaw)
$\boldsymbol{\psi}_i, \boldsymbol{\alpha}_i$ = elastic angular displacement and velocity vectors for component i

I. Introduction

HIGH-ALTITUDE, long-endurance (HALE) unmanned aerial vehicles (UAVs) are recently receiving considerable attention from the technical community. These UAVs are expected to maintain flights at stratospheric atmosphere (with altitudes varying from 17 to 25 km) and to stay aloft for a long duration of time, possibly exceeding NASA's current goal of 14 days. Possible areas of their use vary from surveillance to telecommunications. For example, they can be used in spotting forest fires; tracking hurricanes for predicting their landfall in coastlines; watching disaster sites such as fires, floods, and earthquakes; monitoring borders and coastlines; and, most important, serving as "atmospheric satellites" for relaying telecommunication signals. In the latter area, they are viewed as a good alternative to space satellites, because their launch, operation, and maintenance are significantly easier and less expensive and they yield a more thorough land vision, due to relative closeness to the Earth.

There have been several designs of solar-powered HALE UAVs in the past years; worth mentioning are NASA's Pathfinder, Pathfinder Plus, and Helios, for which the wingspan sizes range from 30.2 to 75.3 m [1]. Between 1997 and 2001, all three prototypes underwent a series of flight tests in Kauai, Hawaii. In August 2001, the Helios prototype reached a record altitude, exceeding 29.5 km [2]. In these tests, the flight durations extended to 18 hours [1]. Also worth mentioning is the European very-long-endurance stratospheric unmanned air vehicle HeliPlat®, which was designed at the Politecnico di Torino in Turin, Italy [3]. A scaled prototype was manufactured and structurally tested under shear-bending-torsion loading up to an ultimate load of $7g$, although flight tests have not been carried out yet. Another HALE UAV currently under development at the Politecnico di Torino is the solar HALE aircraft for multipayload and operations (SHAMPO®) [4], which was found to be the best compromise between performance, surfaces available for solar-cells, and volume for multipayload purposes. Several profiles and wing plans have been analyzed using computational fluid dynamics (CFD) software. A finite element method (FEM) analysis was carried out to predict the static and dynamic behavior of the structure.

The structure of the aircraft described earlier needs to be extremely lightweight and capable of carrying a considerable amount of nonstructural weight such as that due to sensors, actuators, solar cells, and other types of instruments. For low drag (or thrust required), the aircraft must have a high aspect ratio. Moreover, safety margins for unmanned aircraft need not be as high as those for manned aircraft. All of these factors clearly imply that the resulting aircraft is highly flexible, with very low structural frequencies, perhaps in the order of frequencies involved in flight dynamics. Hence, the separation between the elastic and rigid body motions of the aircraft no longer exists, and for the dynamic analysis, a unified approach must be used. Also, for control design, it is important to use an accurate model of aircraft that accounts for both rigid body and elastic motions. A control design that feeds back only the rigid body variables might be coupled with the elastic motions and, in some cases, destabilize the aircraft. A newly developed formulation presented in [5,6] is ideally suited for the analysis and design of such aircraft. It integrates, into a single seamless formulation, pertinent material from analytical dynamics, structural dynamics, aerodynamics, and multivariable control. Based on fundamental principles, the unified formulation incorporates, in a natural manner, both the rigid body motions of the aircraft as a whole and the elastic deformations of the flexible components.

There have been several studies that aim to address the dynamics of HALE UAVs; worth mentioning is the flight dynamics of flexible aircraft presented in [7,8], which has provided good insight into the problem. Patil et al. [9] conducted a nonlinear aeroelastic study on an aircraft model that is geometrically similar to HALE aircraft, with the focus being on the effect of the static structural deflections on the aeroelastic behavior. Patil and Hodges [10] presented a methodology for the analysis of a highly flexible flying wing. The wing is modeled as a geometrically exact beam undergoing large elastic deformations, and the equations are given in terms of intrinsic variables. Shearer and Cesnik [11] presented a framework for analyzing the flight dynamics of highly flexible vehicle configurations that are typically used in HALE aircraft. The formulation couples the nonlinear rigid body equations of motion of the aircraft with the aeroelastic equations that govern its geometrically nonlinear structural response.

The objective of this paper is to develop a dynamic model for the HALE UAV presented in [4] (Fig. 1) and to use the model for stability analysis, control design, and simulation of the aircraft. The next section is devoted to derivation of the equations of motion. A linear elasticity model is assumed so that nonlinearity is only due to rigid body motions and aerodynamics. In Sec. III, a perturbation solution is used to separate the equations into a set of nonlinear differential equations for the *nominal dynamics* and a set of linear differential equations for the *perturbation dynamics* of the aircraft. The nominal dynamics equations are used to design desired flight paths by determining the corresponding trims that include nominal values of control inputs and elastic deformations. Deviations from the nominal dynamics is governed by the perturbation dynamics, which are used in stability analysis, control design, and simulation of the response of the aircraft to initial and external excitations. In the remainder of the paper, the model developed in Secs. II and III will be referred to as a *complete model*. This model will be compared with two frequently used models: 1) the *quasi-rigid aircraft model*, which is the model of the aircraft that is regarded as rigid (Sec. IV) and 2) the *restrained aircraft model*, which is the model of the aircraft with no rigid body degrees of freedom (Sec. V). Section VI outlines the linear quadratic regulator (LQR) method that will be used in the numerical example for control design. The numerical model and the results are presented in Sec. VII. The model of the UAV includes the geometry of the aircraft and mass and flexural and torsional rigidity distributions. The aerodynamic forces and moments will be generated by using lift curve slope and moment and drag coefficients, which are all given for some number of individual strips throughout the aircraft. In the numerical example, the aircraft will be considered in steady level flight at various forward velocities.

The present paper is closely in line with [5,6]. However, it differs from them in two respects:

1) The results in this paper are compared with the quasi-rigid and restrained aircraft models.

2) In the present study, we assume elastic displacements have both nominal and perturbation parts. This allows more accurate determination of the nominal elastic displacements, using the nonlinear nominal dynamics equations.

II. Modeling the Flexible Aircraft

The wing of the aircraft is composed of a left half-wing and a right half-wing that are both modeled as cantilever beams undergoing bending and torsion. The remaining members, namely, vertical and horizontal stabilizers, are assumed to be rigid. In the remainder of the discussion, we will use the subscript r to denote the quantities associated with the right half-wing, l with the left half-wing, h with the horizontal stabilizer, and v with the vertical stabilizer. The motion of the aircraft can be conveniently described by attaching a set of

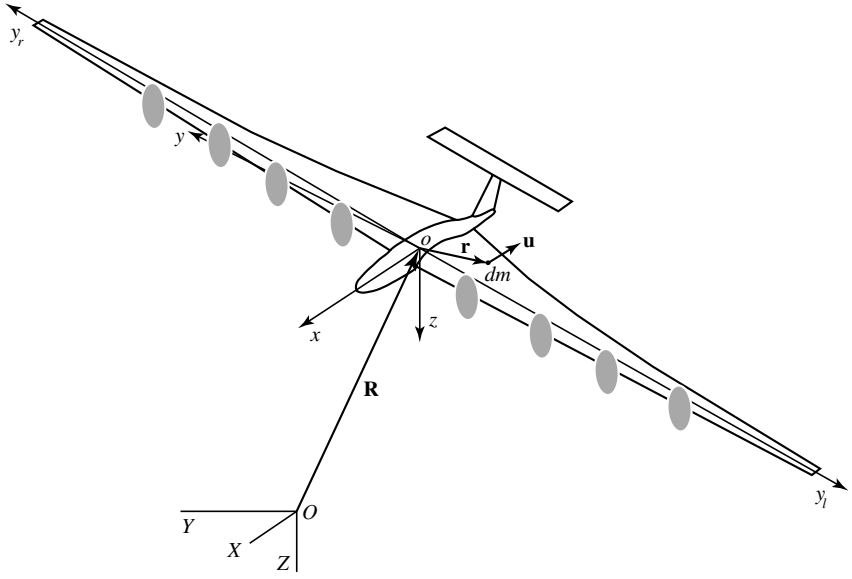

Fig. 1 Flexible HALE UAV.

body axes xyz to the undeformed aircraft at a convenient point, as well as similar body axes to the left and right half-wings (namely, $x_r y_r z_r$ and $x_l y_l z_l$, with origins o_r and o_l, respectively). We assume that the origins o, o_r, and o_l all coincide (Fig. 1). The motion can be expressed by three translations and three rotations of the body axes xyz and elastic deformations of the left and right half-wings, relative to the respective body axes. The generic equations of motion of the whole aircraft are presented in [5], which consist of ordinary differential equations for the rigid body translations and rotations of the aircraft as a whole and the boundary-value problems for the elastic deformations of the wing. For practical reasons, the distributed variables are discretized in space. To this end, we use the Galerkin method and introduce the expansions [5,6]

$$\boldsymbol{u}_i(\boldsymbol{r}_i, t) = \mathrm{U}_i(\boldsymbol{r}_i)\boldsymbol{q}_i(t), \qquad \boldsymbol{\psi}_i(\boldsymbol{r}_i, t) = \Psi_i(\boldsymbol{r}_i)\boldsymbol{\xi}_i(t), \qquad i = r, l \tag{1}$$

where $\boldsymbol{u}_i$ and $\boldsymbol{\psi}_i$ are elastic bending and torsional displacement, respectively; $\boldsymbol{r}_i(x_i, y_i, z_i)$ is a radius vector from o_i to a typical point on the wing; $\mathrm{U}_i(\boldsymbol{r}_i)$ and $\Psi_i(\boldsymbol{r}_i)$ are matrices of shape functions; and $\boldsymbol{q}_i(t)$ and $\boldsymbol{\xi}_i(t)$ are corresponding vectors of generalized coordinates. The shape functions for bending are the eigenfunctions of a uniform cantilever beam; for torsion, they are the eigenfunctions of a uniform clamped-free shaft.

Discrete version of the equations of motion have been obtained in [5] and given as

$$\begin{bmatrix} \dot{\boldsymbol{R}} \\ \dot{\boldsymbol{\theta}} \\ \dot{\boldsymbol{q}}_r \\ \dot{\boldsymbol{q}}_l \\ \dot{\boldsymbol{\xi}}_r \\ \dot{\boldsymbol{\xi}}_l \\ \dot{\boldsymbol{p}}_v \\ \dot{\boldsymbol{\rho}}_\omega \\ \dot{\boldsymbol{p}}_r \\ \dot{\boldsymbol{p}}_l \\ \dot{\boldsymbol{\rho}}_r \\ \dot{\boldsymbol{\rho}}_l \end{bmatrix} = \begin{bmatrix} C^T\boldsymbol{v} \\ E^{-1}\boldsymbol{\omega} \\ \boldsymbol{s}_r \\ \boldsymbol{s}_l \\ \boldsymbol{\eta}_r \\ \boldsymbol{\eta}_l \\ -\tilde{\omega}\boldsymbol{p}_v + \boldsymbol{F} \\ -\tilde{v}\boldsymbol{p}_v - \tilde{\omega}\boldsymbol{\rho}_\omega + \boldsymbol{M} \\ \partial T/\partial \boldsymbol{q}_r - K_r\boldsymbol{q}_r - D_r\boldsymbol{s}_r + \boldsymbol{Q}_r \\ \partial T/\partial \boldsymbol{q}_l - K_l\boldsymbol{q}_l - D_l\boldsymbol{s}_l + \boldsymbol{Q}_l \\ -\mathcal{K}_r\boldsymbol{\xi}_r - \mathcal{D}_r\boldsymbol{\eta}_r + \boldsymbol{\Theta}_r \\ -\mathcal{K}_l\boldsymbol{\xi}_l - \mathcal{D}_l\boldsymbol{\eta}_l + \boldsymbol{\Theta}_l \end{bmatrix} \tag{2}$$

where $\boldsymbol{v} = [u\ v\ w]^T$ and $\boldsymbol{\omega} = [p\ q\ r]^T$ are the vectors of translational and angular velocities of xyz; $\tilde{v}$, and $\tilde{\omega}$ skew symmetric matrices derived from $\boldsymbol{v}$ and $\boldsymbol{\omega}$; C is a matrix of direction cosines between xyz and inertial axes XYZ; $\boldsymbol{R} = [X\ Y\ Z]^T$ is the position vector of the origin o of xyz relative to O of XYZ; E the matrix relating Eulerian velocities to angular quasi velocities; $\boldsymbol{\theta} = [\phi\ \theta\ \psi]^T$ is the symbolic vector of Eulerian angles between xyz and XYZ; $\boldsymbol{F}$ and $\boldsymbol{M}$ are the resultants of gravity, aerodynamic, propulsion, and control force and moment vectors acting on the whole aircraft (in terms of body axes components); K_i and $\mathcal{K}_i$ are the stiffness matrices; D_i and $\mathcal{D}_i$ are the structural damping matrices assumed to be proportional to K_i and $\mathcal{K}_i$, respectively; $\boldsymbol{Q}_i$ and $\boldsymbol{\Theta}_i$ are generalized force vectors, and

$$\boldsymbol{p}_v = \frac{\partial T}{\partial \boldsymbol{v}}, \qquad \boldsymbol{\rho}_\omega = \frac{\partial T}{\partial \boldsymbol{\omega}}; \qquad \boldsymbol{p}_i = \frac{\partial T}{\partial \boldsymbol{s}_i}, \qquad \boldsymbol{\rho}_i = \frac{\partial T}{\partial \boldsymbol{\eta}_i} \qquad i = r, l \tag{3}$$

are the momenta vectors in which T is the kinetic energy. It is clear in Eq. (2) that we assume a linear structural model. However, another study by the authors uses a nonlinear one to capture limit cycle oscillations of HALE wings [12]. The total kinetic energy of the aircraft can be written as a summation of kinetic energies of the individual components, as follows:

$$T = \sum_i T_i, \qquad T_i = \frac{1}{2}\int \bar{\boldsymbol{v}}_i^T \bar{\boldsymbol{v}}_i \, \mathrm{d}m_i, \qquad i = r, l, h, v \tag{4}$$

where $\bar{\boldsymbol{v}}_i$ is the velocity of a typical point in the component i, and $\mathrm{d}m_i$ is the corresponding mass differential element. The velocity can be expressed as

$$\bar{\boldsymbol{v}}_i(\boldsymbol{r}_i, t) = C_i\boldsymbol{v} + (\tilde{r}_i + \widetilde{\mathrm{U}_i\boldsymbol{q}_i})^T C_i\boldsymbol{\omega} + \mathrm{U}_i\boldsymbol{s}_i + \tilde{r}_i^T\Psi_i\boldsymbol{\eta}_i \quad i = r, l; \qquad \bar{\boldsymbol{v}}_i(\boldsymbol{r}_i, t) = \boldsymbol{v} + \tilde{r}_i^T\boldsymbol{\omega}, \quad i = h, v \tag{5}$$

where C_i is the matrix of direction cosines between $x_i y_i z_i$ and xyz ($i = r, l$). Note that the velocities are in their respective body axes. Inserting Eq. (5) into Eq. (4) and carrying out the indicated operations, the total kinetic energy can be written in the compact form:

$$T = \tfrac{1}{2}\boldsymbol{V}^T M \boldsymbol{V} \tag{6}$$

where $\boldsymbol{V} = [\boldsymbol{v}^T\ \boldsymbol{\omega}^T\ \boldsymbol{s}_r^T\ \boldsymbol{s}_l^T\ \boldsymbol{\eta}_r^T\ \boldsymbol{\eta}_l^T]^T$ is the discrete system velocity vector and M is the system mass matrix, which can be expressed in a partitioned form as

$$M = \begin{bmatrix} mI & \tilde{S}^T & C_r^T \int \mathrm{U}_r \,\mathrm{d}m_r & C_l^T \int \mathrm{U}_l \,\mathrm{d}m_l & C_r^T \int \tilde{r}_r^T \Psi_r \,\mathrm{d}m_r & C_l^T \int \tilde{r}_l^T \Psi_l \,\mathrm{d}m_l \\ & J & C_r^T \int \tilde{\chi}_r \mathrm{U}_r \,\mathrm{d}m_r & C_l^T \int \tilde{\chi}_l \mathrm{U}_l \,\mathrm{d}m_l & C_r^T \int \tilde{\chi}_r \tilde{r}_r^T \Psi_r \,\mathrm{d}m_r & C_l^T \int \tilde{\chi}_l \tilde{r}_l^T \Psi_l \,\mathrm{d}m_l \\ & & \int \mathrm{U}_r^T \mathrm{U}_r \,\mathrm{d}m_r & 0 & \int \mathrm{U}_r^T \tilde{r}_r^T \Psi_r \,\mathrm{d}m_r & 0 \\ & & & \int \mathrm{U}_l^T \mathrm{U}_l \,\mathrm{d}m_l & 0 & \int \mathrm{U}_l^T \tilde{r}_l^T \Psi_l \,\mathrm{d}m_l \\ & & \text{symmetric} & & \int \mathrm{U}_r^T \tilde{r}_r \tilde{r}_r^T \Psi_r \,\mathrm{d}m_r & 0 \\ & & & & & \int \mathrm{U}_l^T \tilde{r}_l \tilde{r}_l^T \Psi_l \,\mathrm{d}m_l \end{bmatrix} \tag{7}$$

in which $\tilde{\chi}_i = \tilde{r}_i + \widetilde{\mathrm{U}_i \boldsymbol{q}_i}$, m is the aircraft total mass,

$$\tilde{S} = \sum_{i=r,l} \int C_i^T (\tilde{r}_i + \widetilde{\mathrm{U}_i \boldsymbol{q}_i}) C_i \,\mathrm{d}m_i + \sum_{i=h,v} \int \tilde{r}_i \,\mathrm{d}m_i \tag{8}$$

is the matrix of first moments of inertia of the deformed aircraft, and

$$J = \sum_{i=r,l} \int C_i^T (\tilde{r}_i + \widetilde{\mathrm{U}_i \boldsymbol{q}_i})(\tilde{r}_i + \widetilde{\mathrm{U}_i \boldsymbol{q}_i})^T C_i \,\mathrm{d}m_i + \sum_{i=h,v} \int \tilde{r}_i \tilde{r}_i^T \,\mathrm{d}m_i \tag{9}$$

is the inertia matrix of the deformed aircraft. Denoting the momenta vector for the whole aircraft by $\boldsymbol{p} = [\boldsymbol{p}_v^T \ \boldsymbol{\rho}_\omega^T \ \boldsymbol{p}_r^T \ \boldsymbol{p}_l^T \ \boldsymbol{\rho}_r^T \ \boldsymbol{\rho}_l^T]^T$, we can write

$$\boldsymbol{p} = \frac{\partial T}{\partial \boldsymbol{V}} = M\boldsymbol{V} \tag{10}$$

Note that the relation between $\boldsymbol{p}$ and $\boldsymbol{V}$ is nonlinear because $M = M(\boldsymbol{q}_r, \boldsymbol{q}_l)$. Moreover, we have

$$\frac{\partial T}{\partial \boldsymbol{q}_i} = \frac{\partial \bar{\boldsymbol{v}}_i^T}{\partial \boldsymbol{q}_i} \frac{\partial T}{\partial \bar{\boldsymbol{v}}_i} = -\int \mathrm{U}_i^T \widetilde{C_i \boldsymbol{\omega}} \bar{\boldsymbol{v}}_i \,\mathrm{d}m_i, \qquad i = r, l \tag{11}$$

which includes Coriolis and centrifugal forces for component i.

The generalized forces $\boldsymbol{F}$, $\boldsymbol{M}$, $\boldsymbol{Q}_i$, and $\boldsymbol{\Theta}_i$ ($i = r, l$) are related to the actual forces, which consist of the distributed force $\boldsymbol{f}_i(\boldsymbol{r}_i, t)$ over component i, due to aerodynamics, gravity, and the engine thrust $\boldsymbol{T}$. Note that the engine thrust force can be treated as distributed by writing $\boldsymbol{T}\delta(\boldsymbol{r}_i - \boldsymbol{r}_T)$, where $\delta(\boldsymbol{r}_i - \boldsymbol{r}_T)$ is a spatial Dirac delta function in which $\boldsymbol{r}_T$ denotes the location of the engines. The relation between the generalized forces and the actual forces can be obtained by means of the virtual work. For brevity, we will omit the intermediate steps and present the expressions directly:

$$\begin{aligned} \boldsymbol{F} &= \sum_{i=r,l} C_i^T \int_{D_i} [\boldsymbol{f}_i + \boldsymbol{T}\delta(\boldsymbol{r}_i - \mathbf{r}_T)] \,\mathrm{d}D_i + \sum_{i=h,v} \int_{D_i} \boldsymbol{f}_i \,\mathrm{d}D_i \\ \boldsymbol{M} &= \sum_{i=r,l} C_i^T \int_{D_i} (\tilde{r}_i + \widetilde{\mathrm{U}_i \boldsymbol{q}_i})[\boldsymbol{f}_i + \boldsymbol{T}\delta(\boldsymbol{r}_i - \boldsymbol{r}_T)] \,\mathrm{d}D_i \\ &\quad + \sum_{i=h,v} \int_{D_i} \tilde{r}_i \boldsymbol{f}_i \,\mathrm{d}D_i \\ \boldsymbol{Q}_i &= \int_{D_i} \mathrm{U}_i^T [\boldsymbol{f}_i + \boldsymbol{T}\delta(\boldsymbol{r}_i - \boldsymbol{r}_T)] \,\mathrm{d}D_i, \\ \boldsymbol{\Theta}_i &= \int_{D_i} \Psi_i^T \tilde{r}_i [\boldsymbol{f}_i + \boldsymbol{T}\delta(\boldsymbol{r}_i - \boldsymbol{r}_T)] \,\mathrm{d}D_i, \qquad i = r, l \end{aligned} \tag{12}$$

The engine thrust, aileron angle, elevator angle, and rudder angle enter into the equations of motion [Eq. (2)] through the generalized forces [Eq. (12)].

To generate the distributed aerodynamic forces, a quasi-steady theory and a strip theory will be employed. Distributed force over the right half-wing can be shown to be

$$\boldsymbol{f}_{ar} = \begin{bmatrix} l_r \sin\alpha_r - d_r \cos\alpha_r \\ 0 \\ -l_r \cos\alpha_r - d_r \sin\alpha_r \end{bmatrix} \simeq l_r \begin{bmatrix} \alpha_r \\ 0 \\ -1 \end{bmatrix} - d_r \begin{bmatrix} 1 \\ 0 \\ \alpha_r \end{bmatrix} \tag{13}$$

where

$$\alpha_r = \tan^{-1}(\bar{v}_{rz}/\bar{v}_{rx}) + \psi_{ry} \simeq \bar{v}_{rz}/\bar{v}_{rx} + \psi_{ry} \tag{14}$$

is the local angle of attack and

$$\begin{aligned} l_r &= q_r c_r (C_{L0} + C_{L\alpha}\alpha_r - C_{La}\delta_a) \\ d_r &= q_r c_r (C_{D0} + C_{D\alpha}\alpha_r), \qquad q_r = \tfrac{1}{2}\rho|\bar{\boldsymbol{v}}_r|^2 \end{aligned} \tag{15}$$

are the lift and drag per unit span and the dynamic pressure, respectively.

Note that ψ_{ry} is the angular displacement of the wing about axis y_r, due to torsion. Similarly, aerodynamics distributed force over the left half-wing is

$$\boldsymbol{f}_{al} = \begin{bmatrix} -l_l \sin\alpha_l + d_l \cos\alpha_l \\ 0 \\ -l_l \cos\alpha_l - d_l \sin\alpha_l \end{bmatrix} \simeq l_l \begin{bmatrix} -\alpha_l \\ 0 \\ -1 \end{bmatrix} - d_l \begin{bmatrix} -1 \\ 0 \\ \alpha_l \end{bmatrix} \tag{16}$$

where

$$\begin{aligned} \alpha_l &\simeq -\bar{v}_{lz}/\bar{v}_{lx} - \psi_{ly}, \qquad l_l = q_l c_l (C_{L0} + C_{L\alpha}\alpha_l + C_{La}\delta_a) \\ d_l &= q_l c_l (C_{D0} + C_{D\alpha}\alpha_l), \qquad q_l = \tfrac{1}{2}\rho|\bar{\boldsymbol{v}}_l|^2 \end{aligned} \tag{17}$$

Aerodynamic distributed force for the horizontal tail is

$$\boldsymbol{f}_{ah} \simeq l_h \begin{bmatrix} \alpha_h \\ 0 \\ -1 \end{bmatrix} - d_h \begin{bmatrix} 1 \\ 0 \\ \alpha_h \end{bmatrix} \tag{18}$$

$$\begin{aligned} \alpha_h &\simeq \bar{v}_{hz}/\bar{v}_{hx}, \qquad l_h = q_h c_h (C_{L0} + C_{L\alpha}\alpha_h + C_{Le}\delta_e) \\ d_h &= q_h c_h (C_{D0} + C_{D\alpha}\alpha_h), \qquad q_h = \tfrac{1}{2}\rho|\bar{\boldsymbol{v}}_h|^2 \end{aligned} \tag{19}$$

Finally, the aerodynamic distributed force over the vertical tail can be written as

$$\boldsymbol{f}_{av} = \begin{bmatrix} l_v \sin\alpha_v - d_v \cos\alpha_v \\ -l_v \cos\alpha_v - d_v \sin\alpha_v \\ 0 \end{bmatrix} \simeq l_v \begin{bmatrix} \alpha_v \\ -1 \\ 0 \end{bmatrix} - d_v \begin{bmatrix} 1 \\ \alpha_v \\ 0 \end{bmatrix} \tag{20}$$

$$\begin{aligned} \alpha_v &\simeq \bar{v}_{vy}/\bar{v}_{vx}, \qquad l_v = q_v c_v (C_{L\alpha}\alpha_v + C_{Lr}\delta_r) \\ d_v &= q_v c_v C_{D\alpha}\alpha_v, \qquad q_v = \tfrac{1}{2}\rho|\bar{\boldsymbol{v}}_v|^2 \end{aligned} \tag{21}$$

In what follows, we assume that $C_{Li}\delta_i = \hat{\delta}_i$ and $i = a, e, r$, and we treat $\hat{\delta}_i$ as inputs instead of δ_i.

The gravitational distributed force of the individual components are simply

$$\begin{aligned} \boldsymbol{f}_{gi} &= C_i C_f \begin{bmatrix} 0 \\ 0 \\ m_i g \end{bmatrix}, \qquad i = r, l \\ \boldsymbol{f}_{gi} &= C_f \begin{bmatrix} 0 \\ 0 \\ m_i g \end{bmatrix}, \qquad i = h, v \end{aligned} \tag{22}$$

Note that the aerodynamic and gravity forces are in terms of respective component body axes.

III. Perturbation Solution

The state equations (2) represent a set of nonlinear differential equations for which the order depends on the number of elastic degrees of freedom of the model. The dynamics of such a system can be addressed by adapting a perturbation approach, which amounts to assuming that the quantities can be expressed as the sum of a large part, called the zero-order part, and a small part, called the first-order part, as follows:

$$\begin{aligned} &\boldsymbol{R} = \boldsymbol{R}^0 + \boldsymbol{R}^1, \qquad \boldsymbol{\theta} = \boldsymbol{\theta}^0 + \boldsymbol{\theta}^1, \qquad \boldsymbol{v} = \boldsymbol{v}^0 + \boldsymbol{v}^1 \\ &\boldsymbol{\omega} = \boldsymbol{\omega}^0 + \boldsymbol{\omega}^1 \qquad \boldsymbol{q}_i = \boldsymbol{q}_i^0 + \boldsymbol{q}_i^1, \qquad \boldsymbol{s}_i = \boldsymbol{s}_i^0 + \boldsymbol{s}_i^1 \\ &\boldsymbol{\xi}_i = \boldsymbol{\xi}_i^0 + \boldsymbol{\xi}_i^1, \qquad \boldsymbol{\eta}_i = \boldsymbol{\eta}_i^0 + \boldsymbol{\eta}_i^1, \qquad i = r, l \end{aligned} \tag{23}$$

in which the zero-order quantities, denoted by the superscript 0, are at least one order of magnitude larger than the first-order quantities, denoted by superscript 1. Substituting Eq. (23) into Eq. (2) and separating different orders of magnitude, we get the zero-order equations:

$$\begin{bmatrix} \dot{\boldsymbol{R}}^0 \\ \dot{\boldsymbol{\theta}}^0 \\ \dot{\boldsymbol{q}}_r^0 \\ \dot{\boldsymbol{q}}_l^0 \\ \dot{\boldsymbol{\xi}}_r^0 \\ \dot{\boldsymbol{\xi}}_l^0 \\ \dot{\boldsymbol{p}}_v^0 \\ \dot{\boldsymbol{\rho}}_\omega^0 \\ \dot{\boldsymbol{p}}_r^0 \\ \dot{\boldsymbol{p}}_l^0 \\ \dot{\boldsymbol{\rho}}_r^0 \\ \dot{\boldsymbol{\rho}}_l^0 \end{bmatrix} = \begin{bmatrix} (C^0)^T \boldsymbol{v}^0 \\ (E^0)^{-1} \boldsymbol{\omega}^0 \\ \boldsymbol{s}_r^0 \\ \boldsymbol{s}_l^0 \\ \boldsymbol{\eta}_r^0 \\ \boldsymbol{\eta}_l^0 \\ -\tilde{\omega}^0 \boldsymbol{p}_v^0 + \boldsymbol{F}^0 \\ -\tilde{v}^0 \boldsymbol{p}_v^0 - \tilde{\omega}^0 \boldsymbol{\rho}_\omega^0 + \boldsymbol{M}^0 \\ (\partial T/\partial \boldsymbol{q}_r)^0 - K_r \boldsymbol{q}_r^0 - D_r \boldsymbol{s}_r^0 + \boldsymbol{Q}_r^0 \\ (\partial T/\partial \boldsymbol{q}_l)^0 - K_l \boldsymbol{q}_l^0 - D_l \boldsymbol{s}_l^0 + \boldsymbol{Q}_l^0 \\ -\mathcal{K}_r \boldsymbol{\xi}_r^0 - \mathcal{D}_r \boldsymbol{\eta}_r^0 + \boldsymbol{\Theta}_r^0 \\ -\mathcal{K}_l \boldsymbol{\xi}_l^0 - \mathcal{D}_l \boldsymbol{\eta}_l^0 + \boldsymbol{\Theta}_l^0 \end{bmatrix} \tag{24}$$

for the nominal dynamics and the first-order equations

$$\begin{bmatrix} \dot{\boldsymbol{R}}^1 \\ \dot{\boldsymbol{\theta}}^1 \\ \dot{\boldsymbol{q}}_r^1 \\ \dot{\boldsymbol{q}}_l^1 \\ \dot{\boldsymbol{\xi}}_r^1 \\ \dot{\boldsymbol{\xi}}_l^1 \\ \dot{\boldsymbol{p}}_v^1 \\ \dot{\boldsymbol{\rho}}_\omega^1 \\ \dot{\boldsymbol{p}}_r^1 \\ \dot{\boldsymbol{p}}_l^1 \\ \dot{\boldsymbol{\rho}}_r^1 \\ \dot{\boldsymbol{\rho}}_l^1 \end{bmatrix} = \begin{bmatrix} (C^1)^T \boldsymbol{v}^0 + (C^0)^T \boldsymbol{v}^1 \\ (E^1)^{-1} \boldsymbol{\omega}^0 + (E^0)^{-1} \boldsymbol{\omega}^1 \\ \boldsymbol{s}_r^1 \\ \boldsymbol{s}_l^1 \\ \boldsymbol{\eta}_r^1 \\ \boldsymbol{\eta}_l^1 \\ -\tilde{\omega}^1 \boldsymbol{p}_v^0 - \tilde{\omega}^0 \boldsymbol{p}_v^1 + \boldsymbol{F}^1 \\ -\tilde{v}^1 \boldsymbol{p}_v^0 - \tilde{v}^0 \boldsymbol{p}_v^1 - \tilde{\omega}^1 \boldsymbol{\rho}_\omega^0 - \tilde{\omega}^0 \boldsymbol{\rho}_\omega^1 + \boldsymbol{M}^1 \\ (\partial T/\partial \boldsymbol{q}_r)^1 - K_r \boldsymbol{q}_r^1 - D_r \boldsymbol{s}_r^1 + \boldsymbol{Q}_r^1 \\ (\partial T/\partial \boldsymbol{q}_l)^1 - K_l \boldsymbol{q}_l^1 - D_l \boldsymbol{s}_l^1 + \boldsymbol{Q}_l^1 \\ -\mathcal{K}_r \boldsymbol{\xi}_r^1 - \mathcal{D}_r \boldsymbol{\eta}_r^1 + \boldsymbol{\Theta}_r^1 \\ -\mathcal{K}_l \boldsymbol{\xi}_l^1 - \mathcal{D}_l \boldsymbol{\eta}_l^1 + \boldsymbol{\Theta}_l^1 \end{bmatrix} \tag{25}$$

for the perturbation dynamics of the aircraft. Note that the zero-order quantities that are obtained from the solution of the zero-order equations (24) enter into the first-order equations as inputs. Substituting the perturbation solutions (23) into Eq. (10) and separating the different orders of magnitudes, we obtain

$$\boldsymbol{p}^0 = M^0 \boldsymbol{V}^0 \quad \text{and} \quad \boldsymbol{p}^1 = M^1 \boldsymbol{V}^0 + M^0 \boldsymbol{V}^1 \tag{26}$$

where $M^0 = M^0(\boldsymbol{q}_r^0, \boldsymbol{q}_l^0)$ is the zero-order and $M^1 = M^1(\boldsymbol{q}_r^0, \boldsymbol{q}_l^0, \boldsymbol{q}_r^1, \boldsymbol{q}_l^1)$ is the first-order mass matrix.

The zero-order equations (24) are nonlinear, and a solution to them must also satisfy the zero-order momenta-velocity vector relation, the first of Eqs. (26), which is also nonlinear. Considering how aircraft are flown, the zero-order rigid body variables $[\boldsymbol{R}^0(t), \boldsymbol{\theta}^0(t), \boldsymbol{v}^0(t)$, and $\boldsymbol{\omega}^0(t)]$ representing a desired aircraft maneuver are predefined and, hence, known. The zero-order equations, along with the zero-order momenta-velocity vector relation, are used to determine the required control input $\boldsymbol{u}^0(t)$ and the resulting elastic deflections $\boldsymbol{q}_i^0(t)$ and $\boldsymbol{\xi}_i^0(t)$ and their time derivatives $\boldsymbol{s}_i^0(t)$ and $\boldsymbol{\eta}_i^0(t)$ for $i = r, l$. Noting that $\boldsymbol{R}^0(t)$ does not appear in the equations explicitly, the zero-order equations are time-invariant if $\boldsymbol{\theta}^0$, $\boldsymbol{v}^0$, and $\boldsymbol{\omega}^0$ (representing a desired maneuver) are constant, otherwise, they are time-varying. In steady cases such as steady level flight and steady turn maneuver, the zero-order equations reduce to algebraic equations and a solution can be obtained relatively easily, as demonstrated later in the numerical example.

Solving the second term of Eq. (26) for $\boldsymbol{V}^1$, we have

$$\boldsymbol{V}^1 = (M^0)^{-1}(\boldsymbol{p}^1 - M^1 \boldsymbol{V}^0) \tag{27}$$

Substituting Eq. (27) into the right side of Eq. (25) for $\boldsymbol{V}^1$ and arranging the resulting equations, the first-order equations can be cast in the state-space form:

$$\dot{\boldsymbol{x}}^1(t) = A(t)\boldsymbol{x}^1(t) + B(t)\boldsymbol{u}^1(t) \tag{28}$$

where

$$\boldsymbol{x}^1 = \begin{bmatrix} \boldsymbol{R}^{1T} & \boldsymbol{\theta}^{1T} & \boldsymbol{q}_r^{1T} & \boldsymbol{q}_l^{1T} & \boldsymbol{\xi}_r^{1T} & \boldsymbol{\xi}_r^{1T} & \boldsymbol{p}_v^{1T} & \boldsymbol{\rho}_\omega^{1T} & \boldsymbol{p}_r^{1T} & \boldsymbol{p}_l^{1T} & \boldsymbol{\rho}_r^{1T} & \boldsymbol{\rho}_l^{1T} \end{bmatrix}^T \tag{29}$$

is the first-order state, $\boldsymbol{u}^1$ is the first-order control, and $A(t)$ and $B(t)$ are the coefficient matrices. A and B are time-invariant if $\boldsymbol{\theta}^0$, $\boldsymbol{v}^0$, and $\boldsymbol{\omega}^0$ are constant, otherwise, they are time-varying.

IV. Quasi-Rigid Aircraft

The equations of motion of the aircraft regarded as rigid can be obtained from (2) by collecting the equations corresponding to the rigid body degrees of freedom and setting elastic displacements and velocities to zero. The resulting equations can be written as

$$\begin{bmatrix} \dot{\boldsymbol{R}} \\ \dot{\boldsymbol{\theta}} \\ \dot{\boldsymbol{p}}_v \\ \dot{\boldsymbol{\rho}}_\omega \end{bmatrix} = \begin{bmatrix} C^T \boldsymbol{v} \\ E^{-1} \boldsymbol{\omega} \\ -\tilde{\omega} \boldsymbol{p}_v + \boldsymbol{F} \\ -\tilde{v} \boldsymbol{p}_v - \tilde{\omega} \boldsymbol{\rho}_\omega + \boldsymbol{M} \end{bmatrix} \tag{30}$$

where $\boldsymbol{F}$ and $\boldsymbol{M}$ are obtained from the first two of Eqs. (12) by setting the elastic displacements and velocities to zero. Similar to Eq. (10), the relations between the velocities and the momenta are $\boldsymbol{p}_v = m\boldsymbol{v} + \tilde{S}^T \boldsymbol{\omega}$ and $\boldsymbol{\rho}_\omega = \tilde{S}\boldsymbol{v} + J\boldsymbol{\omega}$, where $\tilde{S}$ and J are the first and second moments of inertia for the quasi-rigid aircraft, which can be obtained from Eqs. (8) and (9) by substituting $\boldsymbol{q}_i = 0$, $i = r, l$. Using these equations to eliminate the momenta, the state equations can be expressed in the compact form:

$$\dot{\boldsymbol{y}}(t) = \boldsymbol{g}[\boldsymbol{y}(t), \boldsymbol{u}(t)] \tag{31}$$

where $\boldsymbol{y} = [\boldsymbol{R}^T \ \boldsymbol{\theta}^T \ \boldsymbol{v}^T \ \boldsymbol{\omega}^T]^T$ is the state vector of order 12, $\boldsymbol{u}$ is the control vector as defined earlier, and $\boldsymbol{g}$ is a nonlinear function of the state and the control vectors.

The control vector $\boldsymbol{u}$ can be chosen so that the aircraft executes a desired maneuver. However, various disturbances cause the aircraft to undergo perturbations from the desired flight path. For stability analysis and feedback control design, we again employ a perturbation approach and write the state as $\boldsymbol{y} = \boldsymbol{y}^0 + \boldsymbol{y}^1$, where $\boldsymbol{y}^1$ is one order of magnitude smaller than $\boldsymbol{y}^0$. Similarly, the control input can also be separated into two parts, namely, $\boldsymbol{u}^0$ and $\boldsymbol{u}^1$. Substituting this solution into Eq. (31), separating terms of different orders of magnitude and ignoring the higher-order terms, we obtain the zero-order state equation:

$$\dot{\boldsymbol{y}}^0(t) = \boldsymbol{g}[\boldsymbol{y}^0(t), \boldsymbol{u}^0(t)] \tag{32}$$

and the first-order, or the perturbation state, equation

$$\dot{\boldsymbol{y}}^1(t) = A_Q(t)\boldsymbol{y}^1(t) + B_Q(t)\boldsymbol{u}^1(t) \tag{33}$$

where $A_Q(t) = A_Q[\boldsymbol{y}^0(t), \boldsymbol{u}^0(t)]$ and $B_Q(t) = B_Q[\boldsymbol{y}^0(t)]$ are the

coefficient matrices. Because $\boldsymbol{y}^0$ and $\boldsymbol{u}^0$ enter into the first-order equation (33) as inputs, Eq. (33) is linear and time-invariant if both $\boldsymbol{y}^0$ and $\boldsymbol{u}^0$ are constant, otherwise, it is time-varying. Once a zero-order state representing a desired maneuver is chosen, the required control input $\boldsymbol{u}^0(t)$ enabling the maneuver can be obtained by solving Eq. (32) for $\boldsymbol{u}^0(t)$.

V. Restrained Aircraft

In this case, the flexible aircraft is assumed to be fixed at the origin o so that it is prevented from undergoing rigid body translations and rotations. The equations of motion for this case can be obtained from Eq. (2) by eliminating the rigid body degrees of freedom, which results in

$$\begin{bmatrix} \dot{\boldsymbol{q}}_i \\ \dot{\boldsymbol{\xi}}_i \\ \dot{\boldsymbol{p}}_i \\ \dot{\boldsymbol{\rho}}_i \end{bmatrix} = \begin{bmatrix} \boldsymbol{s}_i \\ \boldsymbol{\eta}_i \\ \partial T/\partial \boldsymbol{q}_i - K_i \boldsymbol{q}_i - D_i \boldsymbol{s}_i + \boldsymbol{Q}_i \\ -\mathcal{K}_i \boldsymbol{\xi}_i - \mathcal{D}_i \boldsymbol{\eta}_i + \boldsymbol{\Theta}_i \end{bmatrix}, \qquad i = r, l \tag{34}$$

where the quantities are as defined in Eq. (2). Equation (34) is linear and of the order $2n$, where n is the number of elastic degrees of freedom of the whole aircraft. Considering the relation

$$\begin{bmatrix} \boldsymbol{p}_r \\ \boldsymbol{p}_l \\ \boldsymbol{\rho}_r \\ \boldsymbol{\rho}_l \end{bmatrix} = \begin{bmatrix} M_{33} & M_{34} & M_{35} & M_{36} \\ M_{43} & M_{44} & M_{45} & M_{66} \\ M_{53} & M_{54} & M_{55} & M_{56} \\ M_{63} & M_{64} & M_{65} & M_{66} \end{bmatrix} \begin{bmatrix} \boldsymbol{s}_r \\ \boldsymbol{s}_l \\ \boldsymbol{\eta}_r \\ \boldsymbol{\eta}_l \end{bmatrix} \tag{35}$$

where M_{ij} are the respective submatrices of M given in Eq. (7), the preceding equations of motion can be cast in the state-space form:

$$\dot{z}(t) = A_R(t) z(t) \tag{36}$$

where $z = [\boldsymbol{q}_r^T \ \boldsymbol{q}_l^T \ \boldsymbol{\xi}_r^T \ \boldsymbol{\xi}_l^T \ \boldsymbol{s}_r^T \ \boldsymbol{s}_l^T \ \boldsymbol{\eta}_r^T \ \boldsymbol{\eta}_l^T]^T$ is the state vector; and $A_R(t) = A_R[\boldsymbol{y}^0(t), \boldsymbol{u}^0(t)]$ is the coefficient matrix in which $\boldsymbol{y}^0(t)$ is the zero-order state of the quasi-rigid aircraft (representing a desired maneuver), and $\boldsymbol{u}^0(t)$ is the control input vector (enabling the maneuver) obtained as the solution of Eq. (32).

VI. Control Design

Flying aircraft are subjected to various disturbances that tend to drive them from the intended maneuver and to cause vibration. If the system is controllable, these effects can be suppressed through controls, which are carried out by means of the engine thrust and the control surfaces. As indicated in the earlier sections, there are two types of controls, one type designed to permit the aircraft to execute a desired maneuver and the other type designed to reduce any deviations from the maneuver to zero, which amounts to suppressing vibration and perturbations in the rigid body motions of the aircraft.

Equation (28) represents a set of linear equations, and the objective is to find a control vector $\boldsymbol{u}^1(t)$ that drives the state vector $\boldsymbol{x}^1$ to zero. To this end, we consider a linear quadratic regulator in which the objective is to determine an optimal control vector that minimizes the quadratic performance measure:

$$J = \frac{1}{2} \int_0^{t_f} [\boldsymbol{x}^{1T}(t) Q(t) \boldsymbol{x}^1(t) + \boldsymbol{u}^{1T}(t) R(t) \boldsymbol{u}^1(t)] \, \mathrm{d}t \tag{37}$$

where Q is a real symmetric positive semidefinite matrix, R is a real symmetric positive definite matrix, and t_f is the final time. It is shown in [13] that the optimal feedback control vector has the form

$$\begin{aligned} \boldsymbol{u}^1(t) &= -R^{-1}(t) B(t)^T K(t) \boldsymbol{x}^1(t) = -G(t) \boldsymbol{x}^1(t) \\ G(t) &= R^{-1}(t) B(t)^T K(t) \end{aligned} \tag{38}$$

where $K(t)$ is a real symmetric matrix satisfying the transient matrix Riccati equation

$$\dot{K} = -Q - A^T K - KA + KBR^{-1} B^T K, \qquad K(t_f) = 0 \tag{39}$$

a nonlinear equation that must be integrated backward in time from t_f to 0. The LQR problem is considerably simpler when the zero-order solution is constant, such as in steady level flight, and in this case, the coefficient matrices A and B are constant. Then, if the system is controllable, Q and R are constant and the Riccati matrix K approaches a constant value. In this case, Eq. (39) reduces to the algebraic matrix Riccati equation:

$$-Q - A^T K - KA + KBR^{-1} B^T K = 0 \tag{40}$$

which can be solved by means of Potter's algorithm [13], and the gain matrix G becomes constant. The closed-loop equation reduces to one with constant coefficients, or

$$\dot{\boldsymbol{x}}^1(t) = (A - BG) \boldsymbol{x}^1(t) \tag{41}$$

which can be used for response simulation. For a stability analysis, we solve the associated eigenvalue problem $(A - BG - \lambda I)\boldsymbol{x} = \boldsymbol{0}$, where λ is an eigenvalue and $\boldsymbol{x}$ is an eigenvector. The closed-loop system is stable if all the eigenvalues have nonpositive real parts.

VII. Numerical Model and Results

The numerical model of the UAV includes the geometry, mass, and stiffness distributions and aerodynamic data. Mass distribution is given in terms of distributed mass per unit span at some number of points and lumped masses due to avionics, fuel cells, fuel tanks, payload, and engines over the wing and lumped masses over horizontal and vertical stabilizers. Stiffness distribution includes flexural rigidity and torsional rigidity given at some number of points over the wing. The aerodynamic theory used in this paper is the strip theory that uses quasi-steady aerodynamic coefficients to generate aerodynamic distributed forces over the quarter-chord line and moments about it for the all lifting surfaces, including the wing and horizontal and vertical stabilizers. The aerodynamic coefficients are the drag and lift coefficients at zero angle of attack, the drag and lift curve slopes, and the moment coefficients about the quarter-chord line, all given for some number of locations over the lifting surfaces.

In this numerical example, we will use the same C and E matrices used in [6]. The body axes $x_r y_r z_r$ and $x_l y_l z_l$ can be obtained from xyz through a sequence of rotation. For example, $x_r y_r z_r$ for the right half-wing can be obtained through a -0.2484-deg rotation about x to an intermediate set of axes $x'y'z'$ and a 5.15-deg rotation about z' to $x_r y_r z_r$. Hence, the matrix of direction cosines C_r and C_l can be shown to be

$$\begin{aligned} C_r &= \begin{bmatrix} 0.9960 & 0.0897 & -0.0004 \\ -0.0897 & 0.9960 & -0.0043 \\ 0 & 0.0043 & 0.9999 \end{bmatrix} \\ C_l &= \begin{bmatrix} -0.9960 & 0.0897 & 0.0004 \\ -0.0897 & -0.9960 & -0.0043 \\ 0 & -0.0043 & 0.9999 \end{bmatrix} \end{aligned} \tag{42}$$

The aircraft has eight engines, as seen in Fig. 1. We label the thrust from these engines as $\boldsymbol{T}_{l4}, \boldsymbol{T}_{l3}, \ldots, \boldsymbol{T}_{r4}$ and assume that $\boldsymbol{T}_{ij} = [T_{ij} \ 0 \ 0]^T$ (where $i = r, l$ and $j = 1, 2, 3, 4$) in body axes xyz and that $T_{ij}^0 = T^0$ (where $i = r, l$ and $j = 1, 2, 3, 4$) and $\boldsymbol{T}_{rj}^1 = \boldsymbol{T}_{lj}^1 = [T_j^1 \ 0 \ 0]^T$ (where $j = 1, 2, 3, 4$). Hence, the zero-order and the first-order control input vectors will have the forms

$$\boldsymbol{u}^0 = [T^0 \ \hat{\delta}_a^0 \ \hat{\delta}_e^0 \ \hat{\delta}_r^0]^T, \qquad \boldsymbol{u}^1 = [T_1^1 \ T_2^1 \ T_3^1 \ T_4^1 \ \hat{\delta}_a^1 \ \hat{\delta}_e^1 \ \hat{\delta}_r^1]^T \tag{43}$$

We assume that the wing undergoes a bending displacement in the z_i direction and torsion about the y_i axis ($i = r, l$). The shape functions for bending are the eigenfunctions of a uniform cantilever beam:

$$\mathrm{U}_{ij}(y_i) = \sin\beta_j y_i - \sinh\beta_j y_i - \frac{\sin\beta_j\ell + \sinh\beta_j\ell}{\cos\beta_j\ell + \cosh\beta_j\ell}(\cos\beta_j y_i - \cosh\beta_j y_i) \qquad (44)$$

$$i = r, l; \qquad j = 1, 2, \ldots$$

and for torsion, the eigenfunctions of a uniform clamped-free shaft

$$\Psi_{ij}(y_i) = \sin\frac{(2j-1)\pi y_i}{2\ell}, \qquad i = r, l; \qquad j = 1, 2, \ldots \qquad (45)$$

where the length of the half-wing is $\ell = 36.65$ m. In this numerical example, we use two shape functions for both bending and torsion. Using these shape functions, the stiffness matrices are obtained as

$$K_i = \begin{bmatrix} 929.3 & -2640.5 \\ -2640.5 & 19,195.6 \end{bmatrix} \text{N/m}$$
$$\mathcal{K}_i = \begin{bmatrix} 100,686.8 & 186,929.4 \\ 186,929.4 & 595,961.2 \end{bmatrix} \text{Nm/rad}, \qquad i = r, l \qquad (46)$$

For this example, the structural damping matrices are assumed to be zero.

The total mass of the aircraft is $m = 919.5$ kg. For brevity, we will list only the constant parts of $\tilde{S}$ and J as submatrices of the mass matrix M:

$$S = \begin{bmatrix} 0 & 261.9 & 0 \\ -261.9 & 0 & 1437.0 \\ 0 & -1437.0 & 0 \end{bmatrix} \text{kg m}$$
$$J = \begin{bmatrix} 118,484.0 & 0 & -1674.8 \\ 0 & 8557.8 & 0 \\ -1674.8 & 0 & 125,845.0 \end{bmatrix} \text{kg m}^2 \qquad (47)$$

In this part of the example, we consider the aircraft in a steady level flight at $h = 18$ km altitude so that air density is $\rho = 0.12165$ kg/m^3 and speed of sound is $a = 295.07$ m/s. The steady level flight can be prescribed by

$$\boldsymbol{\theta}^0 = \begin{bmatrix} 0 \\ \theta^0 \\ 0 \end{bmatrix}, \qquad \dot{\boldsymbol{R}}^0 = \begin{bmatrix} V_X \\ 0 \\ 0 \end{bmatrix}, \qquad \dot{\boldsymbol{\theta}}^0 = \mathbf{0}$$
$$\boldsymbol{v}^0 = C^0 \begin{bmatrix} V_X \\ 0 \\ 0 \end{bmatrix} = V_X \begin{bmatrix} \cos\theta^0 \\ 0 \\ \sin\theta^0 \end{bmatrix}, \qquad \boldsymbol{\omega}^0 = \mathbf{0} \qquad (48)$$

where V_X is the forward velocity of the aircraft (i.e., the velocity component in the X direction), which is constant. With the preceding choice, the first two of Eqs. (24) are satisfied automatically. Because the elastic displacements are constant in steady level flight, we have $\mathbf{s}_i^0 = 0$ and $\boldsymbol{\eta}_i^0 = 0$, where $i = r, l$, which will satisfy the third through sixth of Eqs. (24). Noting that the time derivatives of momenta are zero, the remaining half of Eqs. (24) can be satisfied by equating the right sides of the equations to zero and solving for the unknowns. Because the aircraft is assumed to be symmetric about the y axis, the force equation in the y direction and the roll and yaw moment equations are satisfied for $\delta_a^0 = \delta_r^0 = 0$. Hence, the aforementioned unknowns for trim are the pitch angle θ^0, the engine thrust T^0, the elevator angle δ_e^0, and the elastic displacements $\boldsymbol{q}_i^0$ and $\boldsymbol{\xi}_i^0$, where $i = r, l$.

The values of these quantities for the complete model are listed in Table 1 in steady level flight for three different forward velocities, $V_X = 40, 50$, and 60 m/s. The trim values for the quasi-rigid aircraft at the same velocities are given in Table 2. The errors made by the quasi-rigid aircraft model in estimating the trim values of θ^0; T^0 and δ_e^0 are higher at lower forward velocities.

Inserting the trim values given in Table 1 into Eq. (25) and arranging the terms, we obtain the A and B matrices of Eq. (28), which are 28×28 and 28×7, respectively. The open-loop eigenvalues (i.e., the eigenvalues when $\boldsymbol{u}^1 = \mathbf{0}$) for each trim case are listed in Table 3, which indicates that the aircraft has four zero eigenvalues for all three trim cases and a positive real eigenvalue for the trim at $V_X = 40$ m/s. Hence, we can conclude that the aircraft is unstable for the case $V_X = 40$ m/s and marginally stable for the cases in which $V_X = 50$ and 60 m/s. Note that the unstable eigenvalue in the table is shown in bold.

The open-loop eigenvalues from the quasi-rigid aircraft model are listed in Table 4, in which λ_5 is the spiral mode; $\lambda_{6,7}$ is the phugoid mode; $\lambda_{8,9}$ is the Dutch roll; $\lambda_{10,11}$ is the short-period mode; and λ_{12} is the rolling convergence mode [14]. The quasi-rigid aircraft has a positive real eigenvalue for the trim at $V_X = 40$ m/s and a pair of complex eigenvalues with a positive real part for both $V_X = 40$ and 50 m/s. Hence, the quasi-rigid aircraft predicts that the aircraft is unstable for both cases. Because this result contradicts with that of the complete model, we conclude that the flexibility has a stabilizing effect in these cases.

Table 1 Trim for the complete model

V_X, m/s	40	50	60
θ^0, rad	0.0039	−0.0262	−0.0425
T^0, N	51.58	72.40	97.92
δ_e^0	−0.3414	−0.2761	−0.2402
$\boldsymbol{q}_r^0$, m	$\begin{bmatrix} -1.0527 \\ -0.1056 \end{bmatrix}$	$\begin{bmatrix} -1.1078 \\ -0.1067 \end{bmatrix}$	$\begin{bmatrix} -1.1722 \\ -0.1076 \end{bmatrix}$
$\boldsymbol{q}_l^0$, m	$\begin{bmatrix} -1.0527 \\ -0.1056 \end{bmatrix}$	$\begin{bmatrix} -1.1078 \\ -0.1067 \end{bmatrix}$	$\begin{bmatrix} -1.1722 \\ -0.1076 \end{bmatrix}$
$\boldsymbol{\xi}_r^0$, rad	$\begin{bmatrix} -0.0045 \\ -0.0011 \end{bmatrix}$	$\begin{bmatrix} -0.0047 \\ -0.0011 \end{bmatrix}$	$\begin{bmatrix} -0.0050 \\ -0.0011 \end{bmatrix}$
$\boldsymbol{\xi}_l^0$, rad	$\begin{bmatrix} -0.0045 \\ -0.0011 \end{bmatrix}$	$\begin{bmatrix} -0.0047 \\ -0.0011 \end{bmatrix}$	$\begin{bmatrix} -0.0050 \\ -0.0011 \end{bmatrix}$

Table 2 Trim for the quasi-rigid aircraft

V_X, m/s	40	50	60
θ^0, rad	0.0024	−0.0279	−0.0443
T^0, N	49.53	70.16	95.42
δ_e^0, rad	−0.3453	−0.2823	−0.2466

Table 3 Eigenvalues of the complete model

V_X, m/s	40	50	60
$\lambda_{1,2,3,4}$	0	0	0
λ_5	**0.0003**	−0.0056	−0.0074
$\lambda_{6,7}$	$-0.0123 \pm 0.2465i$	$0.0146 \pm 0.199i$	$-0.0169 \pm 0.1660i$
$\lambda_{8,9}$	$-0.0423 \pm 0.3493i$	$-0.0501 \pm 0.4316i$	$-0.0599 \pm 0.5149i$
$\lambda_{10,11}$	$-1.9277 \pm 3.6964i$	$-1.9611 \pm 3.8784i$	$-2.2944 \pm 4.1000i$
λ_{12}	$-3.5642 + 2.7053i$	$-4.9116 + 2.0981i$	−5.2338
λ_{13}	$-3.5642 - 2.7053i$	$-4.9116 - 2.0981i$	−6.7345
λ_{14}	−6.2790	−7.8264	−9.3775
$\lambda_{15,16}$	$-2.9153 \pm 10.14i$	$-3.6441 \pm 9.924i$	$-4.3752 \pm 9.654i$
$\lambda_{17,18}$	$-2.4260 \pm 22.54i$	$-2.9995 \pm 22.52i$	$-3.5493 \pm 22.50i$
$\lambda_{19,20}$	$-0.0616 \pm 51.49i$	$-0.0881 \pm 51.58i$	$-0.1217 \pm 51.69i$
$\lambda_{21,22}$	-0.1869 ± 52.79	$-0.2547 \pm 52.92i$	$-0.3361 \pm 53.07i$
$\lambda_{23,24}$	$-2.3351 \pm 70.78i$	$-2.9297 \pm 70.88i$	$-3.5293 \pm 71.00i$
$\lambda_{25,26}$	$-0.0907 \pm 89.67i$	$-0.1043 \pm 89.58i$	$-0.1109 \pm 89.47i$
$\lambda_{27,28}$	$-0.0251 \pm 90.29i$	$-0.0232 \pm 90.25i$	$-0.0162 \pm 90.21i$

Table 4 Eigenvalues of the quasi-rigid aircraft

V_X, m/s	40	50	60
$\lambda_{1,2,3,4}$	0	0	0
λ_5	**0.0011**	−0.0050	−0.0068
$\lambda_{6,7}$	$\mathbf{0.0054 \pm 0.2387i}$	$\mathbf{0.0003 \pm 0.1932i}$	$-0.0037 \pm 0.1609i$
$\lambda_{8,9}$	$-0.0419 \pm 0.3498i$	$-0.0496 \pm 0.4319i$	$-0.0594 \pm 0.5150i$
$\lambda_{10,11}$	$-2.4554 \pm 2.4976i$	$-3.0453 \pm 3.1546i$	$-3.6439 \pm 3.8106i$
λ_{12}	−6.3026	−7.8671	−9.4370

Table 5 Eigenvalues of the restrained aircraft

V_X, m/s	40	50	60
$\lambda_{1,2}$	$-3.4321 \pm 3.4228i$	$-4.2870 \pm 2.4123i$	-3.9517
$\lambda_{3,4}$	$-3.4321 \pm 3.4228i$	$-4.2870 \pm 2.4123i$	-6.34144
$\lambda_{5,6,7,8}$	$-2.7360 \pm 19.6263i$	$-3.4104 \pm 19.534i$	$-4.0814 \pm 19.421i$
$\lambda_{9,10,11,12}$	$-0.0762 \pm 51.62i$	$-0.1094 \pm 51.73i$	$-0.1516 \pm 51.86i$
$\lambda_{13,14,15,16}$	$-0.0437 \pm 88.10i$	$-0.0458 \pm 88.06i$	$-0.0422 \pm 88.01i$

Table 6 Closed-loop eigenvalues

$V_X = 50$ m/s	Quasi-rigid	Rigid body feedback	Full feedback
λ_1	-0.0222	-0.0222	$-0.0357 + 0.0617i$
λ_2	-0.1917	-0.1881	$-0.0357 - 0.0617i$
λ_3	$-0.1221 + 0.3302i$	$-0.1297 + 0.3299i$	-0.0714
λ_4	$-0.1221 - 0.3302i$	$-0.1297 - 0.3299i$	-0.0811
λ_5	-0.4466	-0.4675	-0.1030
λ_6	$-0.3291 + 0.5455i$	-0.5259	-0.1030
λ_7	$-0.3291 - 0.5455i$	$-0.3053 + 0.5050i$	$-0.1123 - 0.2460i$
λ_8	$-0.7900 + 0.8286i$	$-0.3053 - 0.5050i$	$-0.0501 + 0.4316i$
λ_9	$-0.7900 - 0.8286i$	**0.4819 + 1.9954i**	$-0.0501 - 0.4316i$
λ_{10}	$-3.1489 + 3.2512i$	**0.4819 − 1.9954i**	$-1.9610 + 3.8784i$
λ_{11}	$-3.1489 - 3.2512i$	$-3.8770 + 5.4272i$	$-1.9610 - 3.8784i$
λ_{12}	-7.8677	$-3.8770 - 5.4272i$	$-4.9116 + 2.0981i$
λ_{13}		-7.9626	$-4.9116 + 2.0981i$
λ_{14}		-7.9826	-7.8264
$\lambda_{15,16}$		$-3.5547 \pm 10.40i$	$-3.6441 \pm 9.92i$
$\lambda_{17,18}$		$-3.1335 \pm 22.50i$	$-2.9995 \pm 22.52i$
$\lambda_{19,20}$		$-0.1156 \pm 51.58i$	$-0.0881 \pm 51.58i$
$\lambda_{21,22}$		$-0.2508 \pm 52.90i$	$-0.2547 \pm 52.92i$
$\lambda_{23,24}$		$-2.9139 \pm 71.17i$	$-2.9297 \pm 70.88i$
$\lambda_{25,26}$		$-0.1103 \pm 89.59i$	$-0.1043 \pm 89.58i$
$\lambda_{27,28}$		$-0.0279 \pm 90.24i$	$-0.0232 \pm 90.25i$

The eigenvalues from the restrained aircraft model are listed in Table 5. They all have negative real parts, so that this model predicts that the aircraft is asymptotically stable, which is in agreement with the results reported in [4]. However, the results contradict the stability conclusion of the complete model.

Comparing the actual eigenvalues (i.e., the eigenvalues of the complete model) with the eigenvalues of the quasi-rigid and the restrained aircraft models, the coupling between the rigid body and the elastic motions is reflected in all of the eigenvalues and we can no longer label the eigenvalues as "eigenvalues for rigid body motion" and/or "eigenvalues for elastic motion." However, the coupling has more effect on some of the eigenvalues than on others. In general, the eigenvalues with low absolute values are closer to those of quasi-rigid aircraft and the eigenvalues with high absolute values are closer to those of restrained aircraft. The eigenvalues in between possess the largest effect of the coupling.

As listed in Table 3, the aircraft typically has four zero eigenvalues and one very small positive or negative real eigenvalue. Because these eigenvalues are very similar to the first four eigenvalues of the quasi-rigid aircraft, listed in Table 4, one would wonder if it is possible to stabilize the aircraft by designing a feedback control as if the aircraft was rigid (i.e., by feeding back only the rigid body variables using the quasi-rigid dynamics [15]). To explore this, we consider only the trim case for $V_X = 50$ m/s and use the coefficient matrices A_Q and B_Q for the quasi-rigid aircraft obtained earlier (not listed here) and follow the LQR method described in Sec. VI to design a feedback control so that the quasi-rigid aircraft is stable. The control gain matrix is not given here, for brevity. The eigenvalues of the closed-loop quasi-rigid system are listed in the first column of Table 6, and it is clear from these eigenvalues that the quasi-rigid aircraft is stable. Because in this control design we use a full state feedback (not output feedback), we are sure that the controller has some degree of robustness so that it can forgive some variations in the coefficient matrices. This means that the control signal obtained by feeding back the rigid body variables might also stabilize the flexible aircraft. Of course, this will depend on the degree of robustness of the controller and the degree of flexibility of the aircraft. The eigenvalues of the complete model with a feedback control as if the aircraft was rigid are listed in the second column of Table 6. Two of the eigenvalues ($\lambda_{9,10}$) have positive real parts so that the flexible aircraft is unstable. This proves that a feedback control design based on only the quasi-rigid aircraft model can actually destabilize the aircraft, instead of improving its stability.

To stabilize the aircraft, the complete model must be used. As an illustration, we design a full state feedback control based on the complete model using the LQR method for the trim at $V_X = 50$ m/s. The details are not presented here, for brevity. The eigenvalues of the closed-loop system are listed in the last column of Table 6. All of the eigenvalues have negative real parts, contrary to the eigenvalues listed in the second column of Table 6, so that the feedback control successfully stabilizes the system. Next, we simulate the response of the closed-loop system to initial conditions. Initial values for all of the first-order displacements and velocities are assumed to be zero, except the sideslip velocity $v^1(0) = 20$ m/s. Time histories of the significant displacements and velocities are shown in Figs. 2–5. Significant control inputs are the aileron and rudder angles, for which the time histories are shown in Fig. 6. As seen on the left in Fig. 3, the frequency of oscillation of the elastic tip displacement is notably smaller than the frequencies of the restrained aircraft model. Similarly, the torsional tip displacement, shown on the right in Fig. 3, also has small frequency components, in the range of frequencies of the quasi-rigid aircraft rather than of restrained aircraft.

The complete and the restrained aircraft models can also be used for flutter speed prediction. The flutter speed can be defined as the lowest forward velocity V_X of the aircraft in steady level flight at which the coefficient matrix A (or A_R for the restrained aircraft model) has at least one pair of purely imaginary eigenvalues. Flutter speeds for some discrete values of altitudes (varying from sea level to 28 km for both the complete and the restrained aircraft models) are shown in Fig. 7. The flutter frequencies for varying altitudes remain constant at around $\omega_F = 89.63$ rad/s for the complete model and $\omega_F = 87.87$ rad/s for the restrained aircraft model. Note that in

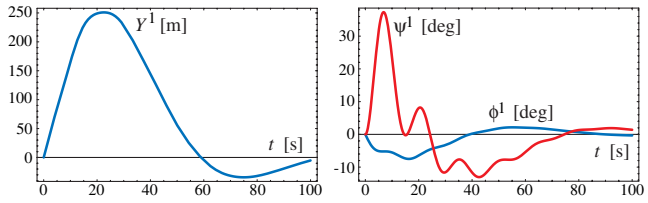

Fig. 2 Rigid body displacements.

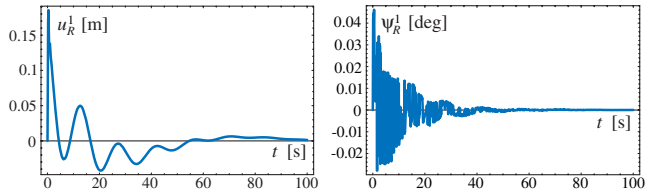

Fig. 3 Elastic tip displacements of the right half-wing.

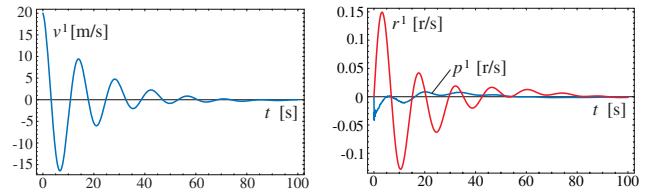

Fig. 4 Rigid body velocities.

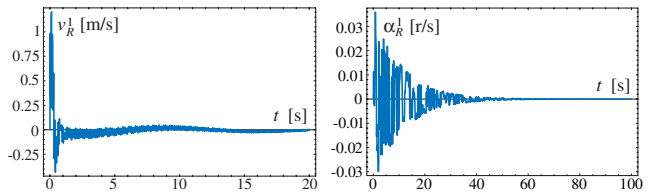

Fig. 5 Elastic tip velocities of the right half-wing.

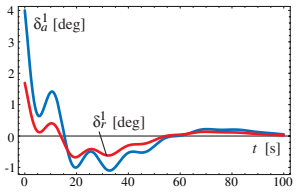

Fig. 6 Aileron and rudder angles.

Fig. 7, each point for the complete model corresponds to certain trim values that are used in computing the corresponding coefficient matrix A. However, at each point for the restrained aircraft model, the quasi-rigid aircraft model is used to compute the trim values and the corresponding A_R matrix is computed based on these trim values. To include the compressibility effect of the flow, the aerodynamic coefficients C_{L0} and $C_{L\alpha}$ are corrected by the compressibility correction factor $1/\sqrt{1-\mathcal{M}^2}$. It is easy to see in Fig. 7 that significant error is made by the restrained aircraft model in predicting the flutter speed for altitudes beyond 17 km. Also, the flutter speed for high altitudes is significantly low, which raises concerns, because this type of aircraft is expected to operate at high altitudes.

VIII. Conclusions

In this paper, the dynamic modeling of a HALE UAV was carried out and the model was used for stability analysis, control design, and simulation of the aircraft. The wing of the aircraft was modeled as flexible and the remaining components were rigid. The equations of motion were a set of first-order nonlinear differential equations. A perturbation approach was used to separate the equations into a set of

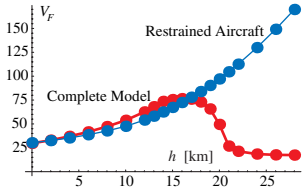

Fig. 7 Flutter speeds.

nonlinear equations for the nominal dynamics and a set of linear equations for the perturbation dynamics. In the numerical example, the maneuver of interest was steady level flight at various forward velocities. The nominal dynamics equations were used to compute required control inputs permitting the flight and the corresponding structural deformations for each of the forward velocities. The stability of the aircraft about the maneuver was addressed by inspecting the eigenvalues of the perturbation equations. The results of the complete model were compared with the results of the quasi-rigid aircraft and the restrained aircraft models. It was shown that a control design based on the quasi-rigid aircraft model might destabilize the aircraft, instead of improving its stability, and that the complete model must be used for a proper feedback control. Moreover, the results indicated that the flutter speed at high altitudes is significantly low and that prediction by the restrained aircraft model is extremely inaccurate, especially at high altitudes.

References

[1] Ehemberger, L. J., Donohue, C., and Teets, E. H., Jr., "A Review of Solar-Powered Aircraft Flight Activity at the Pacific Missile Range Test Facility, Kauai, Hawaii," NASA CASI-2004-0095939, 2004.

[2] Teets, E. H., Jr., Donohue, C. J., Wright, P. T., and DelFrate, J., "Meteorological Support of the Helios World Record High Altitude Flight to 96,863 Feet," NASA TM-2002-210727, 2002.

[3] Romeo, G., Frulla, G., Cestino, E., and Corsino, G., "HELIPLAT: Design, Aerodynamic, Structural Analysis of Long-Endurance Solar-Powered Stratospheric Platform," *Journal of Aircraft*, Vol. 41, No. 6, 2004, pp. 1505–1520.

[4] Romeo, G., Frulla, G., Cestino, E., and Borello, F., "SHAMPO: Solar Hale Aircraft for MultiPayload & Operations," *L'Aerotecnica, Missili e Spazio*, Vol. 85, No. 1, 2006, pp. 24–33.

[5] Meirovitch, L., and Tuzcu, I., "Unified Theory for the Dynamics and Control of Maneuvering Flexible Aircraft," *AIAA Journal*, Vol. 42, No. 4, April 2004, pp. 714–727.

[6] Tuzcu, I., "Dynamics and Control of Flexible Aircraft," Ph.D. Dissertation, Virginia Polytechnic Inst. and Sate Univ., Blacksburg, VA, Dec. 2001.

[7] Cestino, E., "Design of Very-Long Endurance Solar-Powered UAV," Ph.D. Thesis, Aerospace Engineering Dept., Politecnico di Torino, Turin, Italy, Apr. 2006.

[8] Cestino, E., "Design of Solar High Altitude Long Endurance Aircraft for Multi Payload and Operations," *Journal of Aerospace Science and Technology* (submitted for publication).

[9] Patil, M. J., Hodges, D. H., and Cesnik, C. E. S., "Nonlinear Aeroelasticity and Flight Dynamics of High-Altitude Long-Endurance Aircraft," *Journal of Aircraft*, Vol. 38, No. 1, 2001, pp. 88–94.

[10] Patil, M. J., and Hodges, D. H., "Flight Dynamics of Highly Flexible Flying Wings," *Journal of Aircraft*, Vol. 43, No. 6, Nov.–Dec. 2006, pp. 1790–1799.

[11] Shearer, C. M., and Cesnik, C. E. S., "Nonlinear Flight Dynamics of Very Flexible Aircraft," AIAA Atmospheric Flight Mechanics Conference and Exhibit, San Francisco, CA, AIAA Paper 2005-5805, Aug. 2005.

[12] Romeo, G., Frulla, G., Cestino, E., Marzocca, P., and Tuzcu, I., "Non-Linear Aeroelastic Modeling and Experiments of Flexible Wings," 47th AIAA/ASME/ASCE/AHS/ASC Structures, Structural Dynamics, Materials Conference and Exhibit, AIAA Paper 2006-2186, 2006.

[13] Meirovitch, L., *Dynamics and Control of Structures*, Wiley, New York, 1990.

[14] Etkin, B., and Reid, L. D., *Dynamics of Flight*, 3rd ed., Wiley, New York, 1996.

[15] Tuzcu, I., and Meirovitch, L., "Effects of Flexibility on the Stability of Flying Aircraft," *Journal of Dynamic Systems, Measurement, and Control*, Vol. 127, Mar. 2005, pp. 41–49.